CO2 Reduction

Residual Chlorine Induced Cationic Active Species on a Porous Copper Electrocatalyst for Highly Stable Electrochemical CO$_2$ Reduction to C$_{2+}$

Minhan Li, Yuanyuan Ma, Jun Chen, Robert Lawrence, Wei Luo, Marco Sacchi, Wan Jiang, and Jianping Yang*

Abstract: Electrochemical carbon dioxide (CO$_2$) reduction reaction (CO$_2$RR) is an attractive approach to deal with the emission of CO$_2$ and to produce valuable fuels and chemicals in a carbon-neutral way. Many efforts have been devoted to boost the activity and selectivity of high-value multicarbon products (C$_{2+}$) on Cu-based electrocatalysts. However, Cu-based CO$_2$RR electrocatalysts suffer from poor catalytic stability mainly due to the structural degradation and loss of active species under CO$_2$RR condition. To date, most reported Cu-based electrocatalysts present stabilities over dozens of hours, which limits the advance of Cu-based electrocatalysts for CO$_2$RR. Herein, a porous chlorine-doped Cu electrocatalyst exhibits high C$_{2+}$ Faradaic efficiency (FE) of 53.8% at −1.00 V versus reversible hydrogen electrode (V$_{RHE}$). Importantly, the catalyst exhibited an outstanding catalytic stability in long-term electrocatalysis over 240 h. Experimental results show that the chlorine-induced stable cationic Cu^0/Cu$^+$ species and the well-preserved structure with abundant active sites are critical to the high FE of C$_{2+}$ in the long-term run of electrochemical CO$_2$ reduction.

Introduction

Electrochemical CO$_2$ reduction reaction (CO$_2$RR) powered by renewable energy has emerged as a promising technology for sustainable energy storage and atmospheric CO$_2$ reduction. Concurrently, CO$_2$RR process is able to provide fuels and commodity chemicals in a carbon-neutral way.[1] To date, a variety of electrocatalysts have been developed for CO$_2$RR, while the reduction products are highly catalyst-specific.[2] Cu-based materials stand out as a unique category of electrocatalysts for CO$_2$RR because of their capability to convert CO$_2$ into valuable deep reduction products, such as long-chain hydrocarbons and multicarbon oxygenate (C$_{2+}$ products).[3] However, to data, Cu-based CO$_2$RR electrocatalysts suffer from large overpotentials, unsatisfactory selectivity toward C$_{2+}$ products and poor catalytic stability under CO$_2$RR conditions, which impede the application of CO$_2$RR to valuable C$_{2+}$ products. In that, enormous studies have been carried out to improve the activity and FE of C$_{2+}$ products. Various key factors and strategies that can facilitate C−C coupling have been proposed, such as surface roughness,[4] particular facets,[5] grain boundaries,[6] subsurface oxygen and oxidized copper species,[7] alloying and doping strategy,[8] tandem strategy,[9] electrolyte design,[10] and electrolyzer engineering.[11] Apart from activity and selectivity, stability is also a key performance benchmark for Cu-based CO$_2$RR catalysts.[12] However, the stability of Cu-based electrocatalysts in CO$_2$RR, which is particularly important for the commercialization of this technology, remains less investigated across the researches on CO$_2$RR.[13]

To date, different deactivation mechanisms have been put forward on Cu-based CO$_2$RR catalysts, such as poisoning, dissolution, structural degradation, loss of active phases, accumulation of carbonaceous species and reduction of CuO$_x$ species.[13b,14] In general, the vulnerable structure and active sites of the catalysts may change as the reaction proceed, which largely result in the poor stability of Cu-based electrocatalysts in the course of CO$_2$RR. To mitigate the disintegration of structure and the loss of active sites, graphene oxide wrapped and thick CuO$_x$ outer layer protected Cu nanowires showed enhanced stability for both structure and catalytic performance.[15] Recently, a Cu nanowire catalyst was reported to maintain a high selectivity toward C$_2$H$_4$ for over 200 hours of electrocatalysis, pointing out the importance of stable stepped sites that formed through in situ during electrochemical activation.[16] Therefore, it is of great importance to maintain the stability of catalyst structure and active sites for improving the catalytic performance of Cu-based CO$_2$RR electrocatalysts. On the other hand, although the conclusion is still pending, the crucial role of oxidized Cu species for the improvement of C$_{2+}$ production has been widely investigated. Given the positive relevance between

[*] M. H. Li, Dr. Y. Y. Ma, Prof. W. Luo, Prof. W. Jiang, Prof. J. P. Yang
State Key Laboratory for Modification of Chemical Fibers and
Polymer Materials, International Joint Laboratory for Advanced Fiber
and Low-dimension Materials, College of Materials Science and
Engineering, Donghua University
Shanghai 201620 (P. R. China)
E-mail: jianpingyang@dhu.edu.cn

Prof. J. Chen
ARC Centre of Excellence for Electromaterials Science, Intelligent
Polymer Research Institute, Australian Institute of Innovative
Materials, Innovation Campus, University of Wollongong
Wollongong, NSW 2522 (Australia)

Dr. R. Lawrence, Dr. M. Sacchi
Department of Chemistry, University of Surrey (UK)

Prof. W. Jiang, Prof. J. P. Yang
Institute of Functional Materials, Donghua University
Shanghai 201620 (China)

Supporting information and the ORCID identification number(s) for
the author(s) of this article can be found under:
https://doi.org/10.1002/anie.202102606.

oxidized Cu species and C_{2+} production, the stability of oxidized Cu species is important for maintaining high selectivity of C_{2+} products.[17]

To improve selectivity and stability of Cu-based catalysts, the effect of halogen ions has also been investigated, focusing on either constructing unique Cu nanostructures or specifically adsorbed halogen ions on the catalysts surface or specifically adsorbed halogen ions on the catalysts surface.[18] Recent studies showed that the residual I and modified F in the Cu matrix have been demonstrated to boost C_{2+} production through either stabilized Cu^+ species or facilitated intermediates adsorption.[19] In this work, we proposed a halogen stabilization strategy that residual-chlorine in the Cu matrix induced stable active species for CO_2RR. A halogen-containing precursor, $Cu_4(OH)_6FCl$ nanosheets (CuOHFCl NSs), was first synthesized by a facile hydrothermal process and then electrochemically activated to Cl-doped porous Cu catalysts under CO_2RR condition. The catalysts showed high FE of C_{2+} products and suppressed hydrogen evolution reaction (HER). Importantly, the catalysts exhibited an outstanding stability in a long-term electrocatalysis over 240 hours. The stable Cl-induced cationic active sites and the well-preserved structure of catalyst were found to be responsible for the superior catalytic stability.

Results and Discussion

The CuOHFCl NSs were prepared via a facile hydrothermal method. The sapphire powder of as-prepared CuOHFCl NSs can be synthesized at gram-scale in a single hydrothermal synthesis using an autoclave of 100 milliliters (Figure 1a). The X-ray diffraction (XRD) pattern and Rietveld refinement result of the CuOHFCl NSs were shown in Figure 1b ($R_{wp} = 9.63\%$, $R_p = 11.4\%$). The as-prepared CuOHFCl NSs possesses kagome layered structure with Cu^I atoms in the kagome lattice and Cu^{II} atoms between kagome layers (Figure 1c).[20] Scanning electron microscopy (SEM) and transmission electron microscopy (TEM) confirmed the sheet-like morphology of the as-prepared CuOHFCl NSs with a few microns in planar scale and about tens of nanometers in thickness (Figure 1d and Figure S2). Both the high-resolution transmission electron microscopy (HR-TEM) (Figure 1e) and the selective area electron diffraction (SAED) pattern (Figure 1f) pointed out a highly ordered hexagonal crystalline structure. The energy dispersive spectroscopy (EDS) elemental mapping analysis shows the uniform distribution of elemental Cu, Cl, F, and O (Figure 1g–j). The XPS analysis also confirmed the existence of Cl (7.23 at%) and F
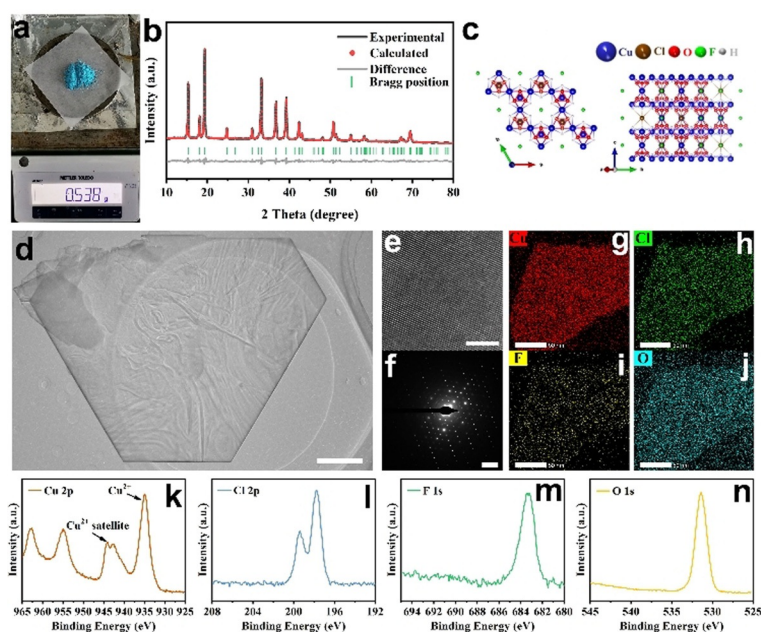
Figure 1. Characterization of as-prepared CuOHFCl NSs. a) Gram-scale CuOHFCl NSs powder obtained in one batch of hydrothermal synthesis in a 100 mL autoclave. b) XRD pattern and Rietveld refinement result of CuOHFCl NSs c) Structural schematic diagrams of CuOHFCl NSs d) TEM image, e) HRTEM, f) SAED pattern, g)–j) elemental mapping, and k)–n) XPS results of as-prepared CuOHFCl NSs. Scale bars: d) 2000 nm. e) 10 nm. f) 5 nm^{-1}. g–j) 50 nm.

(6.61 at%) in the as-prepared CuOHFCl nanosheet (Figure 1k–n and Table S1).

The as-prepared electrode was in situ activated for 10 min at -1.00 V_{RHE} in (denoted as e-CuOHFCl) prior to CO_2RR evaluation. The potential-dependent FEs of gas and liquid products were shown in Figure 2a and b, respectively. The FE of H_2 was suppressed below 30% from -0.75 to -1.00 V_{RHE} with a lowest FE of H_2 of 26.3% at -1.00 V_1, indicating the high selectivity toward CO_2RR. After that, the FE of H_2 gradually increased due to the limited CO_2 mass transfer and intensified HER at more negative potential than -1.00 V_{RHE}.
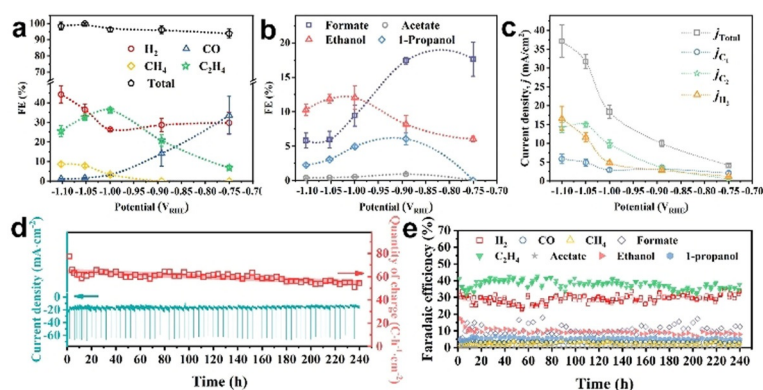
Figure 2. The CO_2RR performance of electrochemical activated e-CuOHFCl nanosheet. a) Potential-dependent FEs of gas phase and total products. b) Potential-dependent FEs of liquid phase products. c) Potential-dependent partial current densities of H_2, C_1, and C_2 and corresponding total current density. d) Current density and quantity of charge in long-term stability test. e) FEs of all products in long-term stability test.

With the reduction potential decreases, CO and formate, as the major C_1 products, showed similar trends and their FE values decreased consistently. The production of CH_4 started at $-1.00\ V_{RHE}$ and the FE of CH_4 was relatively low in the tested range. Therefore, the FE of C_1 products decreased consistently from 51.2% to 15.7% with the decreased potential. The FE of C_2H_4 increased with the decreased potential and reached the peak of 36.3% at $-1.00\ V_{RHE}$. After that, however, the FE of C_2H_4 decreased slightly due to the marked rise in FE of H_2. The liquid C_{2+} products, including ethanol, 1-propanol, and acetate, were detected by ^1H NMR method (Figure S3a,b) and achieved the maximum FEs of 12.0%, 6.1%, and 0.9%, respectively, at -0.89 to $-1.00\ V_{RHE}$. Totally, the FE of C_{2+} products showed a volcano shape with the applied potentials and reached 53.8% at $-1.00\ V_{RHE}$. The total current density, and partial current densities for C_1 and C_{2+} products were shown in Figure 2c. The partial current density for C_{2+} products increased with the decreased applied potentials and reached the maximum of $15.0\ mA\,cm^{-2}$ at $-1.05\ V_{RHE}$. The H_2 partial current density was suppressed below $5.0\ mA\,cm^{-2}$ at potentials above $-1.0\ V_{RHE}$, while it increased significantly at more negative potentials and became the major product at $-1.10\ V_{RHE}$. Interestingly, although the FE of C_1 products showed a significant change with the applied potentials, its partial current density only varied in the range of 2.11 to $5.87\ mA\,cm^{-2}$. Further, if one considered merely the 2 electron transfer products (CO and formate), their partial current densities were almost the same at all applied potentials (Figure S4), which means that the production rates of these two products was nearly constant at all applied potentials.

To explore the effects of halogens and nanosheet morphology on the CO_2RR catalytic performance, two control samples were prepared and tested for CO_2RR under the same condition. $Cu(OH)_2$ nanosheets without halogen elements were prepared by a modified reported method (Figure S5a).[21] Hydrogen accounted for the major reduction product over the activated $Cu(OH)_2$ nanosheets in the range of applied potentials (Figure S5b), while the maximum FE of C_2H_4 products was only 22.7% at $-1.00\ V_{RHE}$ (34.2% for total C_{2+} products). The other control sample was obtained by reducing the CuOHFCl nanosheets in H_2/Ar atmosphere at 350°C for 4 h (denoted as h-CuOHFCl). The nanosheet morphology was destroyed and bulky particles emerged for h-CuOHFCl sample (Figure S5c). The h-CuOHFCl sample also exhibited an inferior catalytic performance compared with CuOHFCl NSs (Figure S5d). H_2 accounted for the major product with FEs ranging from 52.2% to 68.8% over h-CuOHFCl sample, while the maximum FE of C_2H_4 was only 13.3% at $-0.99\ V_{RHE}$. In addition, to exclude the effect of electrochemical surface area (ECSA), double layer capacitance of different catalysts was measured (Figure S6). Considering the higher double layer capacitance values of Cu-$(OH)_2$ NSs and h-CuOHFCl than that of e-CuOHFCl, the partial current density normalized by ECSA of e-CuOHFCl electrocatalyst was even higher than the control samples, indicating its higher intrinsic activity toward C_{2+} products.

The stability was crucial for the application of CO_2RR. Therefore, we carried out consecutive electrocatalysis cycles to determine the long-term CO_2RR stability of e-CuOHFCl catalyst in H-cell at $-1.00\ V_{RHE}$.[16,22] A higher current density was observed for the first electrocatalysis cycle (Figure 2d), which is likely due to the reduction of CuOHFCl to metallic Cu (Figure S7).[22] The rest electrocatalysis cycles showed relatively stable current densities. While the corresponding quantity of charge that passed through the interface of electrode indicated a slight decline in the activity during the whole stability test of 240 h (Figure 2d). The damaged catalyst layer and detached catalyst caused by the stirring and formed bubble is likely responsible for the decreased activity (Figure S8). The FEs of the reduction products during the long-term CO_2RR test were relatively stable without obvious deactivation as shown in Figure 2e (Figure S9 and S10), demonstrating the outstanding catalytic stability of e-CuOHFCl catalyst. To the best of our knowledge, the stability of our catalyst outperforms most reported Cu-based CO_2RR catalysts (Table S2).

To gain an in-depth understanding of the excellent stability of e-CuOHFCl NSs, the electrodes after the stability tests were taken out from catholyte and immediately rinsed with large amount of DI water (the spent catalysts after 4 h and 240 h of CO_2RR are denoted as CuOHFCl-4 and CuOHFCl-240, respectively). The TEM images of the spent catalyst after 4 h of CO_2RR test showed that the CuOHFCl NSs maintained highly porous structure and a sheet-like morphology with roughened surface and edge (Figure 3a). The lattice fringe in the HR-TEM confirmed that the nanosheets were assembled by interconnected metallic Cu grains after reaction (Figure 3b). The HAADF-STEM image and elemental mapping showed that the uniform distribution of Cu, F, and Cl in the porous Cu nanosheets (Figure 3c–f). After stability test of 240 h, the catalysts still possessed the morphology of porous sheet, while the shape of the sheet resembled a leaf of bamboo (Figure 3g and i). Taking a closer look at the tips and edges of the "leaf", the catalyst showed a highly sawtooth edge and layered structure (Figure 3h and Figure S11), which provided abundant stepped and low-coordinated sites that are favorable for the production of C_2 products.[5a, 16, 18b] Furthermore, the elemental mapping demonstrated that Cu, F, and Cl elements were evenly distributed in the spent CuOHFCl-240 sample (Figure 3j–l). Therefore, it is believed that the well-retained porous nanosheet morphology and abundant step sites evolved during the CO_2RR test may contribute to maintain the high FE of C_{2+} products during the long-term stability test.

As shown by the elemental mapping and EDS (Figure S12), F and Cl still existed in the catalysts after CO_2RR stability test. The residual halogens and chemical state of Cu were further examined by XPS spectra after CO_2RR tests. Obviously, a peak corresponding to Cl 2p could be detected on the catalyst after 4 h of CO_2RR test (Figure 4a). In contrast, the absence of Cl 2p peak in $Cu(OH)_2$-CA sample excluded the possible exogenous Cl contamination from the electrolyte or the reference electrode in the cathode cell (Figure 4a). However, after 240 h of CO_2RR test, only a small hump was shown at the position of Cl 2p in the high-resolution Cl XPS spectra (Figure 4a), which may be caused by the detachment of catalyst and the interference of Nafion
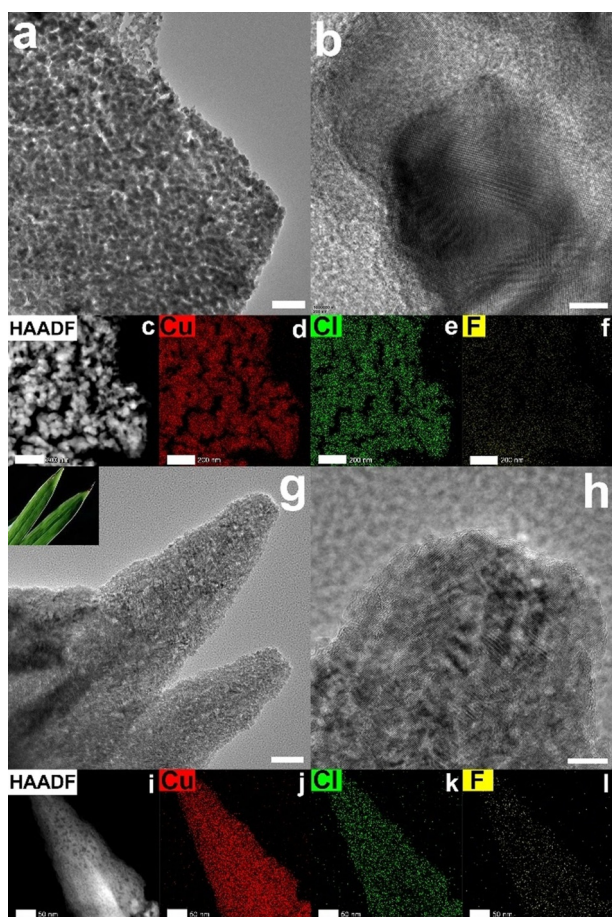
Figure 3. The TEM images and elemental mappings of e-CuOHFCl catalysts at different stages in the long-term stability test. TEM (a,b) and elemental mapping (c–f) after 4 h of electrocatalysis. TEM (g,h) and elemental mapping (i–l) show that the morphology of the catalysts after 240 h of electrocatalysis resemble bamboo leaves (inset in (g)). Scale bars: a) 200 nm. b) 5 nm. c)–f) 200 nm. g) 50 nm. h) 10 nm. i)–l) 50 nm.
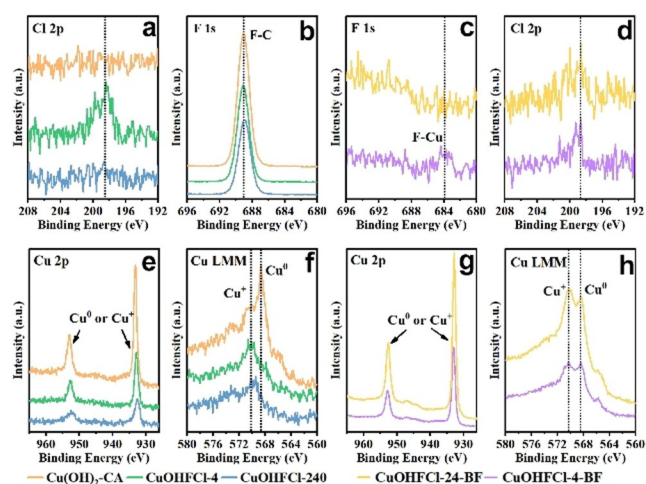
Figure 4. XPS measurements of electrodes after electrocatalysis. Electrodes with Nafion binder: a) Cl 2p. b) F 1s, e) Cu 2p, f) Cu LMM; and electrodes without Nafion binder (Ar sputtered before XPS measurement) c) F 1s, d) Cl 2p, g) Cu 2p, h) Cu LMM.

binder and accumulated adsorbates. Nafion binder is usually used in preparing powdery catalyst inks allowing the strong adhesion between the catalysts and the current collector. However, it imposes difficulty to study the surface properties of the spent electrodes after CO_2RR test as surface-attached Nafion may interfere the XPS characterization, which is evidenced by the ultra intense F-C peak and high F content (Figure 4b. F content: 45–56 at % according to XPS) from Nafion binder (Figure S13). To avoid the interference of Nafion binder, we prepared another two electrodes without Nafion binder and studied their surface properties by XPS after CO_2RR tests at -1.00 V_{RHE} for 4 h and 24 h (denoted as CuOHFCl-4-BF and CuOHFCl-24-BF, BF means binder-free). The electrodes after CO_2RR tests were stored and transferred under inert atmosphere and then in situ Ar sputtered for 300 s before XPS measurements. As shown in the high-resolution XPS spectra of F, the F–C bond disappeared when Nafion was removed demonstrating the successful elimination of the interference from Nafion binder (Figure 4c). A weak peak corresponding to the F-Cu can be observed after 4 h of CO_2RR test,[19a] while no F peaks can be detected after 24 h of CO_2RR test, indicating the gradual leaching of F element as the reaction proceeded. However, different from F, trace amount of Cl element seemed to be relatively stable in the e-CuOHFCl catalyst (Figure 4d), which confirms the Cl residual in the catalyst during the long-term CO_2RR test. The Cu:Cl atomic ratio obtained by XPS measurements before and after 300 s Ar sputtering indicated that Cl existed in both the surface and bulk of the catalysts and the surface Cl content was relatively higher than the bulk (Figure S14 and Table S3). To further investigate the possible residue of halogens in the Cu matrix, we annealed the CuOHFCl NSs by annealing in air and reducing in H_2/Ar atmosphere in a tube furnace, respectively. The thermal gravimetric (TG) analysis showed that the CuOHFCl nanosheets could decompose completely in air at higher than $\approx 445\,°C$ (Figure S15a). The CuOHFCl nanosheets decomposed to CuO after annealing at 500°C in air for 4 h (denoted as a-CuOHFCl, Figure S15b,c). The XPS spectra of F and Cl confirmed the absence of F and the presence of Cl in the a-CuOHFCl sample (Figure S15d,e). Further, the H_2 reduced h-CuOHFCl sample contained a mixed phase of Cu and CuCl (Figure S16a) and the XPS spectra also confirmed the coexistence of Cu^0 and Cu^+ in h-CuOHFCl sample (Figure S16b). Similarly, F was removed while Cl still existed in the h-CuOHFCl sample (Figure S16c,-d). Therefore, although the reason remains unclear, it can be concluded that Cl remained in the Cu matrix of e-CuOHFCl catalysts during CO_2RR test, while F was less stable and leached out in the process of CO_2RR test.

The Cu 2p spectra showed that the chemical state of the catalyst was Cu^0 or Cu^+ after CO_2RR (Figure 4e and g). As it is impossible to distinguish Cu^0 and Cu^+ in the XPS spectra of Cu 2p, the Cu LMM Auger spectra was measured (Figure 4f and h).[12] Based on the peak position of Cu LMM spectra at ≈ 570.1 eV, the predominating copper species on the surface of CuOHFCl-4 and CuOHFCl-240 catalysts were Cu^+ after CO_2RR test.[23] For comparison, a halogen-free $Cu(OH)_2$ nanosheet sample was prepared and tested for CA at the

same potentials as CuOHFCl nanosheets.[21b] The Cu LMM spectra of Cu(OH)$_2$ nanosheets after CA test (denoted as Cu(OH)$_2$-CA) showed a sharp peak at ≈ 568.6 eV, indicating the overwhelming metallic Cu^0 sites on the surface of Cu(OH)$_2$-CA sample. It should be noted that the ex situ XPS has limited capability to probe the surface state of Cu as metallic copper is prone to be oxidized once exposing to air. Although we tried to isolate electrodes after CO$_2$RR tests from air, the surface oxidization seems to be inevitable. However, the quite different predominate Cu LMM Auger peaks in e-CuOHFCl and Cu(OH)$_2$-CA implied the different oxidation state in these two samples. As discussed above, to eliminate the interference of Nafion binder, the Cu LMM Auger spectra were measured on the electrodes without Nafion binder after 4 h and 24 h of CO$_2$RR tests. Further, Ar sputtering was used prior XPS measurement to remove surface layer on the catalysts that was possibly oxidized or contaminated. According to the split peak, it was shown that the mixed oxidation state of Cu^0 and Cu$^+$ existed in the binder-free catalysts under CO$_2$RR condition (Figure 4h).[24] Previously, the crucial role of Cu$^+$ sites or mixed Cu^0-Cu$^+$ sites for the production of C$_{2+}$ products has been widely demonstrated by both theoretical and experimental studies.[12,17b,25] Various strategies have been developed for the purpose of construction and stabilization of Cu$^+$ or mixed Cu^0-Cu$^+$ sites, such as hydroxide/oxide-derived Cu-based catalysts,[7d] plasma treatments,[25b] doping strategies,[8a,26] ligand stabilization,[23b] core–shell structures,[17c,27] and spatial confinement strategy.[17a] Therefore, the stability of cationic Cu sites (Cu$^+$ or mixed Cu^0-Cu$^+$) is crucial to maintain the catalytic performance of Cu-based electrocatalysts.[7c,18b,23a]

Discussion

Halogen doping and oxidation of Cu

The effects of halogen ions on the Cu-based CO$_2$RR electrocatalysts have been widely investigated. On one hand, the halogen ions play an important role in constructing Cu-based nanostructures and stabilizing cation Cu species.[18a,28] The electropolished Cu foil evolved into quite different Cu nanostructures when immerged or electrochemically anodized in halogen-containing solutions, including KCl, KBr, and KI.[10,18b] The unique nanostructures and advantageous facets of cuprous halides derived Cu electrocatalysts was believed to play a significant role for enhanced C$_{2+}$ selectivity.[18a] On the other hand, halogen ions in electrolyte that strongly adsorb on the surface of Cu catalysts could influence the surface charge property as well as the binding strength of certain intermediates.[18e,29] The addition of I$^-$ ions into the CsHCO$_3$ electrolyte was proposed to contribute to the stabilization of Cu$^+$ species under CO$_2$RR reaction by adsorbed iodine ions.[30] Similarly, the use of KCl electrolyte was also demonstrated to induce a biphasic Cu$_2$O-Cu catalyst and preserve Cu$^+$ species under CO$_2$RR.[31] Some works demonstrated the chemical effect of adsorbed halogen ions prevailed over the nanostructuring effect when both effects

jointly contribute to Cu-based electrocatalysts in CO$_2$RR.[10,32]

Although copper halides derived Cu-based electrocatalysts have been widely studied, the effects of residual halogens in Cu matrix remains unclear. Luna and co-workers found that no chlorine remained on the surface of the sol-gel copper oxychloride (Cu$_2$(OH)$_3$Cl) derived catalysts after CO$_2$RR reaction.[17b] However, Vasileff and co-workers revealed that trace amount of iodine species on the iodide-derived copper catalysts, which altered the oxidation state of adjacent Cu sites and favored the C$_2$ production.[19b] Recently, a F modified Cu catalysts derived from Cu(OH)F precursor was fabricated and F was found to boost the C$_{2+}$ production through a hydrogen-assisted C−C coupling mechanism.[19a]

In this work, the Cl ions were found to be more stable than F ions in the e-CuOHFCl electrocatalysts under CO$_2$RR conditions and the residual Cl still existed after long-term CO$_2$RR test. The heteroatomic doping in Cu matrix can induce the change in chemical state and electronic structure of Cu via electron transfer between Cu atoms and the doped atoms.[33] Non-metallic elements, including nitrogen and boron, have also been demonstrated to modify the electronic structure of Cu and induce positively charged Cu sites.[8a,26] The residual I ions also promoted a high content of Cu$^+$ species in iodine-modified Cu catalyst after CO$_2$RR.[18b] Given the larger electronegativity of Cl (3.16) than the other doped heteroatoms in Cu matrix, such as Ag (1.93), B (2.04), N (3.04), and I (2.66), it is reasonable to deduce that mixed oxidation state of Cu^0 and Cu$^+$ in e-CuOHFCl electrocatalyst is likely caused by the residual Cl in Cu matrix. This conception is also supported by the lack of Cu$^+$ species in the halogen-free control sample of Cu(OH)$_2$ after CO$_2$RR, which showed inferior FE of C$_{2+}$ compared to e-CuOHFCl. Therefore, it is believed that the synergistic effects between Cu$^+$ and Cu^0, which were stabilized by residual Cl in e-CuOHFCl electrocatalysts after CO$_2$RR, favored the production of C$_{2+}$ products.[7b,25a] Furthermore, the stable Cu^0-Cu$^+$ sites during the long-term stability test are partly responsible for the excellent catalytic stability.

Stability

The catalytic stability is as important as activity and selectivity for catalysis. However, the studies on the catalytic stability of Cu-based CO$_2$RR electrocatalysts are far from enough to understand the degradation mechanisms and propose the stabilization strategies. In the limited stability studies, the loss of well-defined facets and the changes in the morphology change and structure are major reasons for the decreased activity and selectivity.[34] Cu nanocubes with preferential Cu(100) facet have been proved to be efficient for C−C coupling in CO$_2$RR.[5a,35] However, the nanocubic structure tended to deteriorate under CO$_2$RR condition via a nanoclustering and coalescence mechanism.[36] The evanescence of advantageous Cu(100) facet and increased amount of formed small nanoclusters that favored the HER, which led to the degradation of CO$_2$RR.[34a,36] Similarly, the coarsen of the dendritic Cu nanostructures in the course of CO$_2$RR

resulted in the loss of high index facets, which was believed to be responsible for the degradation of catalytic performance.[13a, 14a] A recent study demonstrated that a thicker and smoother Cu_xO protective layer obtained by controlled surface oxidation could inhibit the disintegration of Cu nanowires and improve its catalytic stability to more than 22 h.[15b] In this study, it was demonstrated that abundant active sites that were induced under CO_2RR conditions were well-retained even after 240 h of electrocatalysis, which may be due to the thermodynamical stability of these active sites under CO_2RR conditions.[16] The well-preserved sheet-like morphology with porous and layered structure would also facilitate the exposure of active sites. On the other hand, it was found that the copper oxidation state changed with the applied potentials as well as the time under reaction conditions.[17b] In this context, the stability of cationic Cu species (Cu^+ or Cu^0-Cu^+) are also of great importance for the catalytic stability in CO_2RR.[17a,25b] Therefore, it is believed that the mixed oxidation state of Cu^0-Cu^+ caused by the residual Cl atoms in e-CuOHFCl electrocatalyst is the key to maintain a stable FE of C_{2+} products in long-term CO_2RR. Based on the above analysis, it is proposed that the stable Cu^0-Cu^+ active sites as well as the integrate structure of the catalysts collectively ensure the outstanding stability of e-CuOHFCl electrocatalysts in CO_2RR.

Conclusion

To summarize, we have proposed a strategy to achieve high selective and stable Cu-based electrocatalysts for CO_2RR through residual-chlorine induced stable active species. A novel porous Cl doped Cu electrocatalyst derived from electrochemically activated CuOHFCl NSs was synthesized. The e-CuOHFCl electrocatalysts exhibited a high FE of C_{2+} products of 53.8% at -1.00 V_{RHE} and a large partial current for C_{2+} products of 15 mA cm^{-2} at -1.05 V_{RHE}. The Cl element was found to be more stable than F element in derived e-CuOHFCl electrocatalysts and remained stable in the Cu matrix under CO_2RR conditions. The residual Cl induced Cu^0-Cu^+ sites as well as favorable morphology of the e-CuOHFCl electrocatalysts were found to boost the C_{2+} production. Importantly, the e-CuOHFCl electrocatalyst presented an outstanding catalytic stability for CO_2RR over 240 h. The residual-chlorine induced stable Cu^0-Cu^+ sites and structural stability of the catalyst were found to be critical to maintain the high FE of C_{2+} in the long-term run of CO_2RR. This study demonstrates new strategies to improve the catalytic stability of Cu-based CO_2RR electrocatalysts.

Acknowledgements

Conflict of interest

The authors declare no conflict of interest.

[1] a) P. De Luna, C. Hahn, D. Higgins, S. A. Jaffer, T. F. Jaramillo, E. H. Sargent, *Science* **2019**, *364*, eaav3506; b) D. Higgins, C. Hahn, C. Xiang, T. F. Jaramillo, A. Z. Weber, *ACS Energy Lett.* **2019**, *4*, 317–324; c) G. Zhu, R. Guo, W. Luo, H. K. Liu, W. Jiang, S. X. Dou, J. Yang, *Natl. Sci. Rev.* **2021**, *8*, nwaa152; d) G. Zhu, F. Zhang, X. Li, W. Luo, L. Li, H. Zhang, L. Wang, Y. Wang, W. Jiang, H. K. Liu, S. X. Dou, J. Yang, *Angew. Chem. Int. Ed.* **2019**, *58*, 6669–6673; *Angew. Chem.* **2019**, *131*, 6741–6745.

[2] a) A. Vasileff, C. Xu, Y. Jiao, Y. Zheng, S.-Z. Qiao, *Chem* **2018**, *4*, 1809–1831; b) N. Han, P. Ding, L. He, Y. Li, Y. Li, *Adv. Energy Mater.* **2020**, *10*, 1902338; c) M. Li, H. Wang, W. Luo, P. C. Sherrell, J. Chen, J. Yang, *Adv. Mater.* **2020**, *32*, 2001848; d) H. Xu, J. Wu, W. Luo, Q. Li, W. Zhang, J. Yang, *Small* **2020**, *16*, 2001775.

[3] a) Y. Zheng, A. Vasileff, X. Zhou, Y. Jiao, M. Jaroniec, S.-Z. Qiao, *J. Am. Chem. Soc.* **2019**, *141*, 7646–7659; b) D. Gao, R. M. Arán-Ais, H. S. Jeon, B. Roldan Cuenya, *Nat. Catal.* **2019**, *2*, 198–210.

[4] a) L. Wang, S. Nitopi, A. B. Wong, J. L. Snider, A. C. Nielander, C. G. Morales-Guio, M. Orazov, D. C. Higgins, C. Hahn, T. F. Jaramillo, *Nat. Catal.* **2019**, *2*, 702–708; b) K. Jiang, Y. Huang, G. Zeng, F. M. Toma, W. A. Goddard, A. T. Bell, *ACS Energy Lett.* **2020**, *5*, 1206–1214.

[5] a) K. Jiang, R. B. Sandberg, A. J. Akey, X. Liu, D. C. Bell, J. K. Nørskov, K. Chan, H. Wang, *Nat. Catal.* **2018**, *1*, 111–119; b) C. Hahn, T. Hatsukade, Y.-G. Kim, A. Vailionis, J. H. Baricuatro, D. C. Higgins, S. A. Nitopi, M. P. Soriaga, T. F. Jaramillo, *Proc. Natl. Acad. Sci. USA* **2017**, *114*, 5918–5923.

[6] a) Z. Chen, T. Wang, B. Liu, D. Cheng, C. Hu, G. Zhang, W. Zhu, H. Wang, Z.-J. Zhao, J. Gong, *J. Am. Chem. Soc.* **2020**, *142*, 6878–6883; b) A. Verdaguer-Casadevall, C. W. Li, T. P. Johansson, S. B. Scott, J. T. McKeown, M. Kumar, I. E. L. Stephens, M. W. Kanan, I. Chorkendorff, *J. Am. Chem. Soc.* **2015**, *137*, 9808–9811.

[7] a) X. Chang, Y. Zhao, B. Xu, *ACS Catal.* **2020**, *10*, 13737–13747; b) S.-C. Lin, C.-C. Chang, S.-Y. Chiu, H.-T. Pai, T.-Y. Liao, C.-S. Hsu, W.-H. Chiang, M.-K. Tsai, H. M. Chen, *Nat. Commun.* **2020**, *11*, 3525; c) W. Zhang, C. Huang, Q. Xiao, L. Yu, L. Shuai, P. An, J. Zhang, M. Qiu, Z. Ren, Y. Yu, *J. Am. Chem. Soc.* **2020**, *142*, 11417–11427; d) Y. Lum, J. W. Ager, *Angew. Chem. Int. Ed.* **2018**, *57*, 551–554; *Angew. Chem.* **2018**, *130*, 560–563.

[8] a) Y. Zhou, F. Che, M. Liu, C. Zou, Z. Liang, P. De Luna, H. Yuan, J. Li, Z. Wang, H. Xie, H. Li, P. Chen, E. Bladt, R. Quintero-Bermudez, T.-K. Sham, S. Bals, J. Hofkens, D. Sinton, G. Chen, E. H. Sargent, *Nat. Chem.* **2018**, *10*, 974–980; b) T. T. H. Hoang, S. Verma, S. Ma, T. T. Fister, J. Timoshenko, A. I. Frenkel, P. J. A. Kenis, A. A. Gewirth, *J. Am. Chem. Soc.* **2018**, *140*, 5791–5797.

[9] a) C. Chen, Y. Li, S. Yu, S. Louisia, J. Jin, M. Li, M. B. Ross, P. Yang, *Joule* **2020**, *4*, 1688–1699; b) C. G. Morales-Guio, E. R. Cave, S. A. Nitopi, J. T. Feaster, L. Wang, K. P. Kuhl, A. Jackson,

N. C. Johnson, D. N. Abram, T. Hatsukade, C. Hahn, T. F. Jaramillo, *Nat. Catal.* **2018**, *1*, 764–771.

[10] D. Gao, F. Scholten, B. Roldan Cuenya, *ACS Catal.* **2017**, *7*, 5112–5120.

[11] D. S. Ripatti, T. R. Veltman, M. W. Kanan, *Joule* **2019**, *3*, 240–256.

[12] S. Y. Lee, H. Jung, N.-K. Kim, H.-S. Oh, B. K. Min, Y. J. Hwang, *J. Am. Chem. Soc.* **2018**, *140*, 8681–8689.

[13] a) N. Martić, C. Reller, C. Macauley, M. Löffler, B. Schmid, D. Reinisch, E. Volkova, A. Maltenberger, A. Rucki, K. J. J. Mayrhofer, G. Schmid, *Adv. Energy Mater.* **2019**, *9*, 1901228; b) S. Popović, M. Smiljanić, P. Jovanovič, J. Vavra, R. Buonsanti, N. Hodnik, *Angew. Chem. Int. Ed.* **2020**, *59*, 14736; *Angew. Chem.* **2020**, *132*, 14844.

[14] a) C. Reller, R. Krause, E. Volkova, B. Schmid, S. Neubauer, A. Rucki, M. Schuster, G. Schmid, *Adv. Energy Mater.* **2017**, *7*, 1602114; b) Z. Gu, N. Yang, P. Han, M. Kuang, B. Mei, Z. Jiang, J. Zhong, L. Li, G. Zheng, *Small Methods* **2019**, *3*, 1800449; c) Z. Weng, X. Zhang, Y. Wu, S. Huo, J. Jiang, W. Liu, G. He, Y. Liang, H. Wang, *Angew. Chem. Int. Ed.* **2017**, *56*, 13135–13139; *Angew. Chem.* **2017**, *129*, 13315–13319.

[15] a) Y. Li, F. Cui, M. B. Ross, D. Kim, Y. Sun, P. Yang, *Nano Lett.* **2017**, *17*, 1312–1317; b) Z. Lyu, S. Zhu, M. Xie, Y. Zhang, Z. Chen, R. Chen, M. Tian, M. Chi, M. Shao, Y. Xia, *Angew. Chem. Int. Ed.* **2021**, *60*, 1909–1915.

[16] C. Choi, S. Kwon, T. Cheng, M. Xu, P. Tieu, C. Lee, J. Cai, H. M. Lee, X. Pan, X. Duan, W. A. Goddard, Y. Huang, *Nat. Catal.* **2020**, *3*, 804–812.

[17] a) P.-P. Yang, X.-L. Zhang, F.-Y. Gao, Y.-R. Zheng, Z.-Z. Niu, X. Yu, R. Liu, Z.-Z. Wu, S. Qin, L.-P. Chi, Y. Duan, T. Ma, X.-s. Zheng, J. Zhu, H.-J. Wang, M.-R. Gao, S.-H. Yu, *J. Am. Chem. Soc.* **2020**, *142*, 6400–6408; b) P. De Luna, R. Quintero-Bermudez, C.-T. Dinh, M. B. Ross, O. S. Bushuyev, P. Todorović, T. Regier, S. O. Kelley, P. Yang, E. H. Sargent, *Nat. Catal.* **2018**, *1*, 103–110; c) Z.-Q. Liang, T.-T. Zhuang, A. Seifitokaldani, J. Li, C.-W. Huang, C.-S. Tan, Y. Li, P. De Luna, C. T. Dinh, Y. Hu, Q. Xiao, P.-L. Hsieh, Y. Wang, F. Li, R. Quintero-Bermudez, Y. Zhou, P. Chen, Y. Pang, S.-C. Lo, L.-J. Chen, H. Tan, Z. Xu, S. Zhao, D. Sinton, E. H. Sargent, *Nat. Commun.* **2018**, *9*, 3828.

[18] a) H. Wang, E. Matios, C. Wang, J. Luo, X. Lu, X. Hu, W. Li, *Nano Lett.* **2019**, *19*, 3925–3932; b) D. Gao, I. Sinev, F. Scholten, R. M. Arán-Ais, N. J. Divins, K. Kvashnina, J. Timoshenko, B. Roldan Cuenya, *Angew. Chem. Int. Ed.* **2019**, *58*, 17047–17053; *Angew. Chem.* **2019**, *131*, 17203–17209; c) T. Kim, G. T. R. Palmore, *Nat. Commun.* **2020**, *11*, 3622; d) S. Verma, X. Lu, S. Ma, R. I. Masel, P. J. A. Kenis, *Phys. Chem. Chem. Phys.* **2016**, *18*, 7075–7084; e) S. A. Akhade, I. T. McCrum, M. J. Janik, *J. Electrochem. Soc.* **2016**, *163*, F477–F484.

[19] a) W. Ma, S. Xie, T. Liu, Q. Fan, J. Ye, F. Sun, Z. Jiang, Q. Zhang, J. Cheng, Y. Wang, *Nat. Catal.* **2020**, *3*, 478–487; b) A. Vasileff, Y. Zhu, X. Zhi, Y. Zhao, L. Ge, H. M. Chen, Y. Zheng, S.-Z. Qiao, *Angew. Chem. Int. Ed.* **2020**, *59*, 19649–19653; *Angew. Chem.* **2020**, *132*, 19817–19821.

[20] R. W. Smaha, W. He, J. M. Jiang, J. Wen, Y.-F. Jiang, J. P. Sheckelton, C. J. Titus, S. G. Wang, Y.-S. Chen, S. J. Teat, A. A. Aczel, Y. Zhao, G. Xu, J. W. Lynn, H.-C. Jiang, Y. S. Lee, *npj Quantum Mater.* **2020**, *5*, 23.

[21] a) J.-J. Lv, M. Jouny, W. Luc, W. Zhu, J.-J. Zhu, F. Jiao, *Adv. Mater.* **2018**, *30*, 1803111; b) L. Jiang, K. Liu, S.-F. Hung, L. Zhou, R. Qin, Q. Zhang, P. Liu, L. Gu, H. M. Chen, G. Fu, N. Zheng, *Nat. Nanotechnol.* **2020**, *15*, 848–853.

[22] M. Rahaman, K. Kiran, I. Z. Montiel, V. Grozovski, A. Dutta, P. Broekmann, *Green Chem.* **2020**, *22*, 6497–6509.

[23] a) J. Kim, W. Choi, J. W. Park, C. Kim, M. Kim, H. Song, *J. Am. Chem. Soc.* **2019**, *141*, 6986–6994; b) N. Sakamoto, Y. F. Nishimura, T. Nonaka, M. Ohashi, N. Ishida, K. Kitazumi, Y. Kato, K. Sekizawa, T. Morikawa, T. Arai, *ACS Catal.* **2020**, *10*, 10412–10419.

[24] G.-F. Chen, Y. Yuan, H. Jiang, S.-Y. Ren, L.-X. Ding, L. Ma, T. Wu, J. Lu, H. Wang, *Nat. Energy* **2020**, *5*, 605–613.

[25] a) H. Xiao, W. A. Goddard, T. Cheng, Y. Liu, *Proc. Natl. Acad. Sci. USA* **2017**, *114*, 6685–6688; b) H. Mistry, A. S. Varela, C. S. Bonifacio, I. Zegkinoglou, I. Sinev, Y.-W. Choi, K. Kisslinger, E. A. Stach, J. C. Yang, P. Strasser, B. R. Cuenya, *Nat. Commun.* **2016**, *7*, 12123.

[26] Z. Yin, C. Yu, Z. Zhao, X. Guo, M. Shen, N. Li, M. Muzzio, J. Li, H. Liu, H. Lin, J. Yin, G. Lu, D. Su, S. Sun, *Nano Lett.* **2019**, *19*, 8658–8663.

[27] L. Shang, X. Lv, H. Shen, Z. Shao, G. Zheng, *J. Colloid Interface Sci.* **2019**, *552*, 426–431.

[28] Y. Kwon, Y. Lum, E. L. Clark, J. W. Ager, A. T. Bell, *ChemElectroChem* **2016**, *3*, 1012–1019.

[29] D. L. T. Nguyen, M. S. Jee, D. H. Won, H.-S. Oh, B. K. Min, Y. J. Hwang, *Catal. Commun.* **2018**, *114*, 109–113.

[30] D. Gao, I. T. McCrum, S. Deo, Y.-W. Choi, F. Scholten, W. Wan, J. G. Chen, M. J. Janik, B. Roldan Cuenya, *ACS Catal.* **2018**, *8*, 10012–10020.

[31] S. Lee, D. Kim, J. Lee, *Angew. Chem. Int. Ed.* **2015**, *54*, 14701–14705; *Angew. Chem.* **2015**, *127*, 14914–14918.

[32] A. S. Varela, W. Ju, T. Reier, P. Strasser, *ACS Catal.* **2016**, *6*, 2136–2144.

[33] X. Lv, L. Shang, S. Zhou, S. Li, Y. Wang, Z. Wang, T.-K. Sham, C. Peng, G. Zheng, *Adv. Energy Mater.* **2020**, *10*, 2001987.

[34] a) P. Grosse, D. Gao, F. Scholten, I. Sinev, H. Mistry, B. Roldan Cuenya, *Angew. Chem. Int. Ed.* **2018**, *57*, 6192–6197; *Angew. Chem.* **2018**, *130*, 6300–6305; b) S. Y. Lee, S. Y. Chae, H. Jung, C. W. Lee, D. L. T. Nguyen, H.-S. Oh, B. K. Min, Y. J. Hwang, *J. Mater. Chem. A* **2020**, *8*, 6210–6218.

[35] N.-T. Suen, Z.-R. Kong, C.-S. Hsu, H.-C. Chen, C.-W. Tung, Y.-R. Lu, C.-L. Dong, C.-C. Shen, J.-C. Chung, H. M. Chen, *ACS Catal.* **2019**, *9*, 5217–5222.

[36] J. Huang, N. Hörmann, E. Oveisi, A. Loiudice, G. L. De Gregorio, O. Andreussi, N. Marzari, R. Buonsanti, *Nat. Commun.* **2018**, *9*, 3117.